Lithos 254–255 (2016) 118–130

Contents lists available at ScienceDirect

Lithos

journal homepage: www.elsevier.com/locate/lithos

Apatite trace element and halogen compositions as petrogenetic-metallogenic indicators: Examples from four granite plutons in the Sanjiang region, SW China

Li-Chuan Pan [a,b], Rui-Zhong Hu [a,*], Xin-Song Wang [a], Xian-Wu Bi [a], Jing-Jing Zhu [a], Chusi Li [c]

[a] State Key Laboratory of Ore Deposit Geochemistry, Institute of Geochemistry, Chinese Academy of Sciences, Guiyang 550002, China
[b] University of Chinese Academy of Sciences, Beijing 100049, China
[c] Department of Geological Sciences, Indiana University, Bloomington, IN 47405, USA

ARTICLE INFO

Article history:
Received 24 September 2015
Accepted 17 March 2016
Available online 1 April 2016

Keywords:
Apatite
REE
Halogens
Oxidation state
Adakite
Ore genesis

ABSTRACT

The abundances of trace elements including Sr, Ga and rare earth elements (REE) and halogens in apatite crystals from four intermediate-felsic plutons in the Zhongdian terrane in the Sanjiang region have been determined using electron microprobe and laser ablation inductively coupled plasma mass spectrometry to evaluate the potential of apatite as a petrogenic-metallogenic indicator. The selected plutons include one that is not mineralized (the Triassic Xiuwacu pluton, or the TXWC pluton), one that hosts a porphyry-type Cu deposit (the Pulang pluton, or the PL pluton), one that hosts a porphyry-type Mo deposit (the Tongchanggou pluton, or the TCG pluton), and one that hosts a vein-type Mo deposit (the Cretaceous Xiuwacu pluton, or the CXWC pluton). Except for the CXWC pluton, the other three plutons have adakite-like trace element signatures in whole rocks. The results from this study show that REE, Sr and halogens in apatite can be used to track magma compositions, oxidation states and crystallization history. Apatite crystals from the adakite-like plutons are characterized by much higher Sr/Y and δEu than the non-adakite-type pluton. This means that apatite, which is not susceptible to alteration, is a useful tool for identifying the adakite-like plutons that no longer preserve the initial Sr/Y ratios in whole rocks due to weathering and hydrothermal alteration. Based on apatite Ga contents and δEu values, it is inferred that the parental magmas for the two adakite-like plutons containing porphyry-type Cu and Mo mineralization are more oxidized than that for the non-adakite-type pluton containing vein-type Mo mineralization. Apatite crystals from the vein-type Mo deposit have much lower Cl/F ratios than those from the porphyry-type Cu and Mo deposits. Apatite crystals from the adakite-like pluton without Cu or Mo mineralization is characterized by much lower Cl/F ratios than those from the adakite-like plutons that host the porphyry-type Cu and Mo deposits. The results from this study confirm the apatite is a useful petrogenetic indicator as well as mineral exploration tool.

1. Introduction

Apatite is an important accessory mineral in granite rocks and is a sink for whole-rock P and some rare earth elements (REE) and halogens (Ayers and Watson, 1993; Henerson, 1980; Nagasawa, 1970; Roeder et al., 1987; Warner et al., 1998; Wass et al., 1980). Experiments covering a wide variety of melt compositions, pressure and temperatures (e.g. Harrison and Watson, 1984; Jahnke, 1984; London et al., 1999; Pichavant et al., 1992; Watson, 1979, 1980; Wolf and London, 1994, 1995) have shown that the solubility of apatite in magma decreases with decreasing temperature and increasing polymerization of magma. Therefore, apatite may appear as an early phase on liquidus in non-peraluminous magma (Harrison and Watson, 1984). In view of its stability, which is not susceptible to hydrothermal alteration and metamorphism (Ayers and Watson, 1991; Creaser and Gray, 1992; Ekstrom, 1972), apatite could record and preserve information on parental magma.

Particularly, halogen compositions in apatite have been applied to estimate contents of F, Cl and H_2O in liquid and melt and speculate voliatite saturation according to the changes of halogens ratios(e.g. Boudreau and Kruger, 1990; Boudreau and McCallum, 1989; Boyce and Hervig, 2009; Boyce et al., 2010; Cawthorn, 1994; Elkins-Tanton and Grove, 2011; Meurer and Boudreau, 1996; Schisa et al., 2015; Warner et al., 1998). Trace elements in apatite such as Mn, Sr, LREE, Th, Y, Eu and Ce have been used to indicate magma composition and oxidation state (e.g. Belousova et al., 2001, 2002; Cao et al., 2012; Piccoli and Candela, 2002; Sha and Chappell, 1999; Tepper and Kuehner, 1999).Moreover, $^{87}Sr/^{86}Sr$ of apatite could record initial $^{87}Sr/^{86}Sr$ values in systems providing an additional approach to trace magmatic process

* Corresponding author. Tel.: +86 851 5891962; fax: +86 851 5891664.
E-mail address: huruizhong@vip.gyig.ac.cn (R.-Z. Hu).

http://dx.doi.org/10.1016/j.lithos.2016.03.010
0024-4937/

and source (e.g. Creaser and Gray, 1992; Tsuboi, 2005; Tsuboi and Suzuki, 2003; Zhang et al., 2011) In addition, apatites have also been traditionally used for U-Th-Pb dating (e.g. Chew et al., 2011; Corfu and Stone, 1998; Gaweda et al., 2014).

Thus, apatite could be a reliable petrogenic-metallogenic indicator (Belousova et al., 2002; Boudreau, 1993; Coulson et al., 2001; Imai, 2004; Martin and John, 1998; Roegge et al., 1974; Treloar and Colley, 1996; Williams and Cesbron, 1977). To test its applicability and explore some new findings, we have selected four granitic intrusions with various types of mineralization and without mineralization in the Zhongdian arc terrane, a major ore deposits cluster of porphyry-type and hydrotherm-type deposits, in the Sanjiang region in Yunnan, SW China. Although previous studies focusing of these plutons and relevant deposits have determined diagenetic and metallogenic ages, the magma and ore-forming material source and fluid properties (e.g. Leng et al., 2007, 2014, Li et al., 2007, 2014, Wang et al., 2014a, 2014b, Yu and Li, 2014, Zeng et al., 2006), it is still an uncertainty for different properties of magmas formed in different epochs and tectonic background and their metallogenic specificity. The results of our study reported in this paper resolve these issues, which confirm that apatite is not only a reliable petrogenetic indicator but also a useful exploration tool.

2. Geological background and samples

The Yidun arc is situated between the Songpan-Garzê Fold Belt and the Qiangtang Block of the eastern Tibetan Plateau. The Yidun arc formed as a result of westward subduction of the Garzê-Litang oceanic plate beneath the Zhongza-Zhongdian micro-continental block (Hou, 1993; Li et al., 2007). The Garzê-Litang Ocean formed from Middle to Late Paleozoic by rifting between the Zhongza-Zhongdian block and the Yangtze craton. Oceanic subduction beneath the Zhongza-Zhongdian block in Late Triassic produced the "Indosinian" granodiorite plutons and associated porphyry-type mineral deposits. In late "Yanshanian", the region underwent post-collisional extension. Partial melting of the continental crust in response to regional decompression produced the Yanshanian granitoids and associated porphyry-type or hydrothermal vein-type mineral deposits.

Four intermediate-felsic plutons in the Zhongza-Zhongdian terrane are selected for this study (Fig. 1). Two of them belong to the Indosinian arc magmatism: the Pulang pluton (PL) and the Triassic Xiuwacu pluton (TXWC). The former hosts a porphyry-type Cu deposit whereas the latter does not. The other two selected plutons belong to the Yanshanian post-collisional magmatism: the Cretaceous Xiuwacu pluton (CXWC)

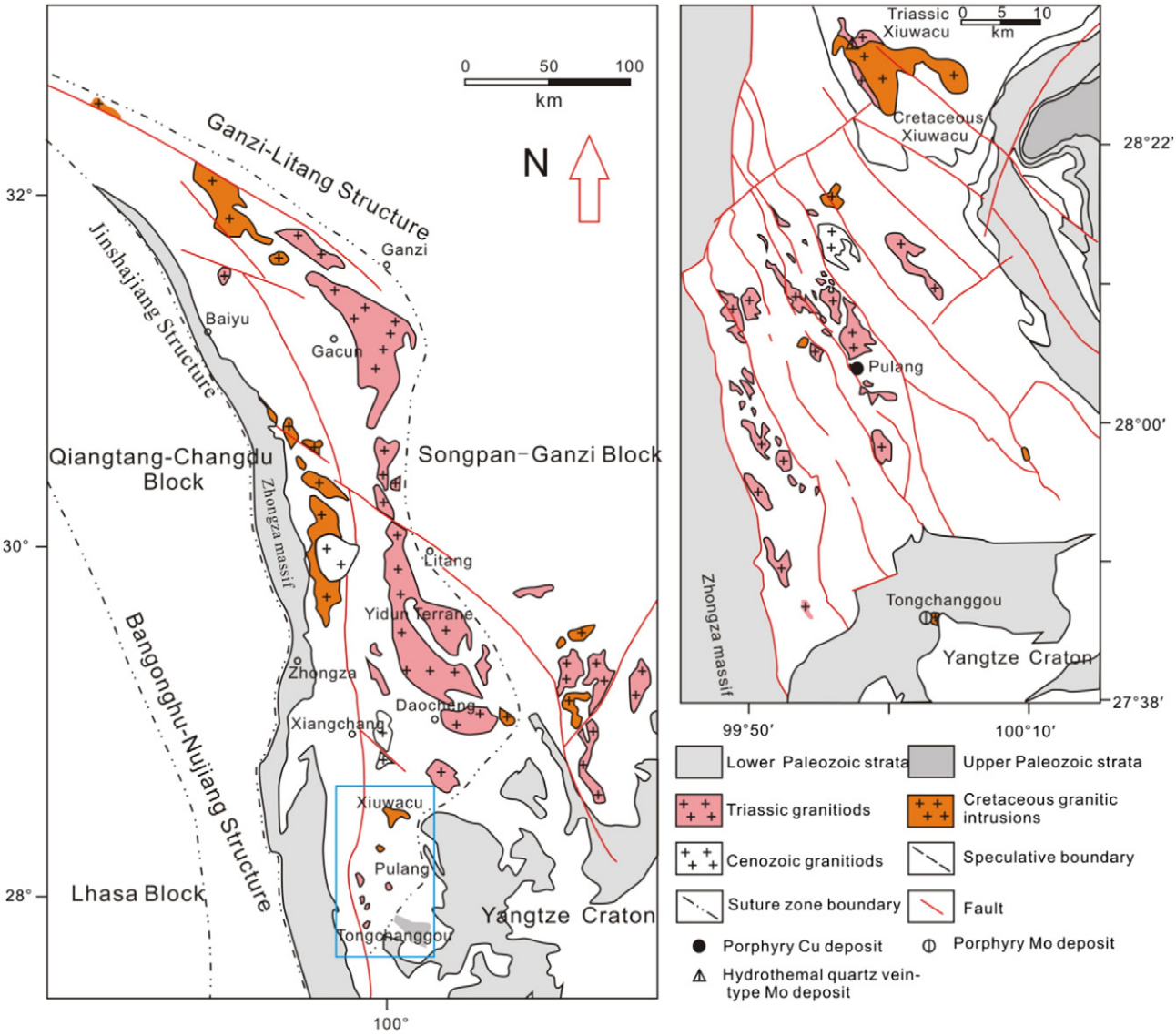

Fig. 1. Regional geological map of the research area, part of the details are based on Wang et al. (2014a). It shows the location of (a) the Yidun arc and (b) the relevant intrusions and deposits.

and the Tongchanggou pluton (TCG) (Fig. 1). The former hosts a quartz vein-type Mo deposit whereas the latter hosts a porphyry-type Mo deposit. The features of ore deposit geology were described in detail by previous studies (Li, 2007; Li et al., 2014; Wang et al., 2014a, 2014b, 2015; Yu et al., 2015). Based on the geological features, geochronology and isotopic geochemistry of the granites and mineralization, those researches confirmed their genetic associations.

3. Petrology

3.1. The Cretaceous Xiuwacu pluton

The CXWC pluton is located ~80 km northwest of Shangri-La city. This pluton is zoned. It consists of three intrusive phases: biotite granite, monzogranite and alkali-feldspar leucogranite (Fig. 2). Apatite is present and most common in the biotite granite and monzogranite units. The apatite grains are mostly euhedral crystals surrounded by feldspar, quartz, biotite and allanite (Fig. 5a,b).

Biotite granite is gray medium- to coarse-grained. K-feldspar, plagioclase, quartz and biotite are the major phases. Accessory phases include apatite, sphene, allanite, zircon and fluorite. Monzogranite is gray medium- to coarse-grained, with smaller amounts of biotite and plagioclase than biotite granite. K-feldspar phenocrysts occur locally in monzogranite, producing a porphyritic texture. Mo mineralization, which occurs in the quartz veins within the pluton, is composed of molybdenite, scheelite, bismuthinite, wolframite and tennantite. Zircon U–Pb age of the host pluton is ~85 Ma (Wang et al., 2014a, 2014b).

Major and trace element compositions of whole rock samples from the CXWC pluton are listed in Appendix 1. The results show that these rocks are metaluminous and calc-alkaline granitoids, with Rittmann index of 2.2–2.4 and A/CNK of 0.99–1.00. These rocks are depleted in Ba, Sr, P and Ti (Fig. 6b) and enriched in light REE relative to heavy REE (Fig. 6a), with $(La/Yb)_N$ ratios of 6.7–21 and pronounced negative Eu anomaly ($Eu/Eu^* < 0.6$). Previous studies show that this pluton is characterized by whole rock $(^{87}Sr/^{86}Sr)_i$ from 0.7075 to 0.7085, and $\varepsilon Nd(t)$ from −6.9 to −7.6, and $\delta^{18}O$ from 5.9‰ to 8.4‰ (Wang et al., 2014b).

3.2. The Tongchanggou pluton

The TCG pluton is located ~15 km southeast of Shangri-La city. Biotite granitic porphyry is the main intrusive phase (Fig. 3). Plagioclase, biotite and quartz occur as phenocrysts; in addition, the matrix also contains K-feldspar and Fe-Mg silicate minerals. The accessory minerals include apatite, sphene, zircon and allanite. Apatite occurs as euhedral crystals surrounded by feldspar and biotite (Fig. 5c,d). The TCG deposit is a porphyry–skarn Mo deposit with skarn-type mineralization in the shallower depths than porphyry-type mineralization. Molybdenite and chalcopyrite are the most important ore minerals.

The zircon U–Pb age of the TCG pluton is ~87 Ma (Wang et al., 2014a). Major and trace element compositions of whole rock samples from the pluton are listed in Appendix 1. The samples are metaluminous and calc-alkaline granitoids with Rittmann index of 2.3 and 2.4 and A/CNK of 0.94 and 0.95. They are depleted in Ba, Nb, Ta and Ti (Fig. 6d), enriched in light REE relative to heavy REE (Fig. 6c), with $(La/Yb)_N = 39.6$ and 40.10 and $Eu/Eu^* = 0.96$ and 1.01. Previous studies show that the pluton is characterized by $(^{87}Sr/^{86}Sr)_i = 0.7069$ and $\varepsilon Nd(t)$ from −5.3 to −5.6 (Wang, 2014c; Wang et al., 2014b).

3.3. The Pulang pluton

The PL pluton is located ~36 km northeast of Shangri-La city. It is composed of quartz diorite porphyrite, quartz monzonitic porphyry and granodiorite porphyry (Fig. 4). Major mineralization is associated with quartz monzonitic porphyry, which is composed of K-feldspar, plagioclase, biotite and quartz as phenocrysts and a matrix containing fine-grained plagioclase, K-feldspar, quartz, biotite and Fe-Mg silicate minerals. The accessory minerals in this rock include apatite, sphene and zircon. Apatite occurs as euhedral crystals surrounded by feldspar and biotite (Fig. 5e,f). The mineralized porphyry unit shows alteration zones that are common in typical porphyry Cu deposits worldwide (Corbett and Leach, 1998; Lowell and Guilbert, 1970). The Cu mineralization in the PL pluton is closely associated with the biotite and K-feldspar alteration zones. Major ore minerals include chalcopyrite, bornite, covellite, galena and molybdenite.

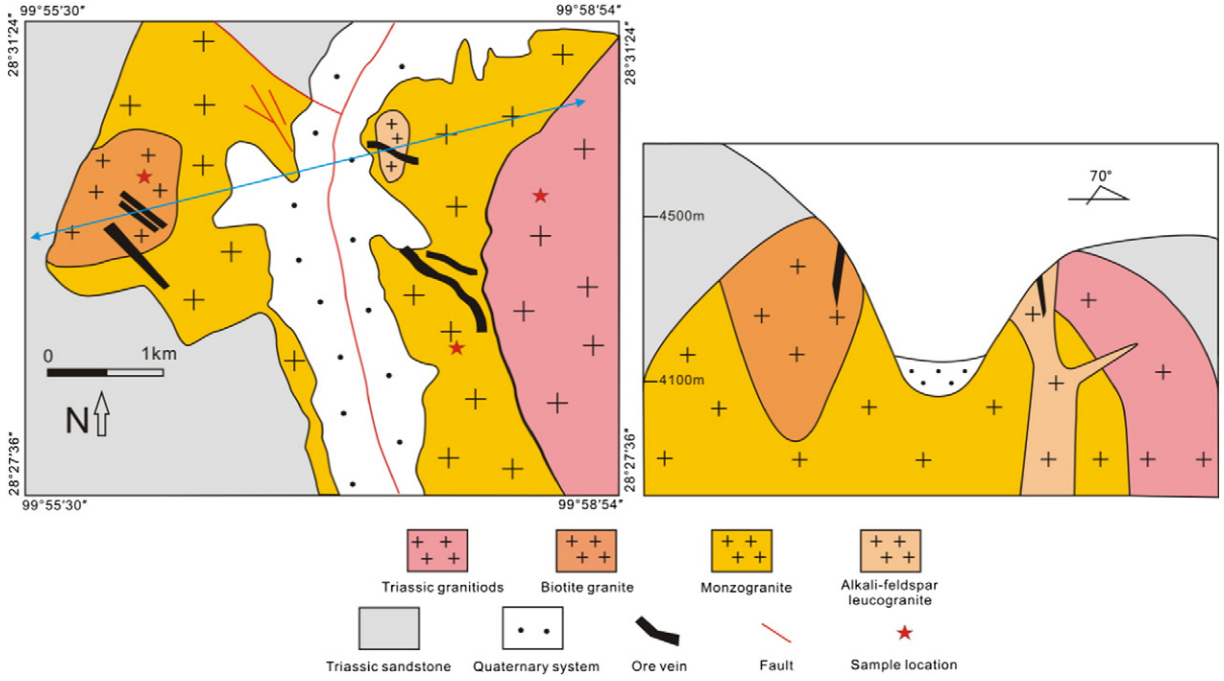

Fig. 2. Simplified geological map and cross-section of the Cretaceous and Triassic Xiuwacu pluton and the associated hydrothermal vein-type Mo deposit modified after Wang et al. (2014b).

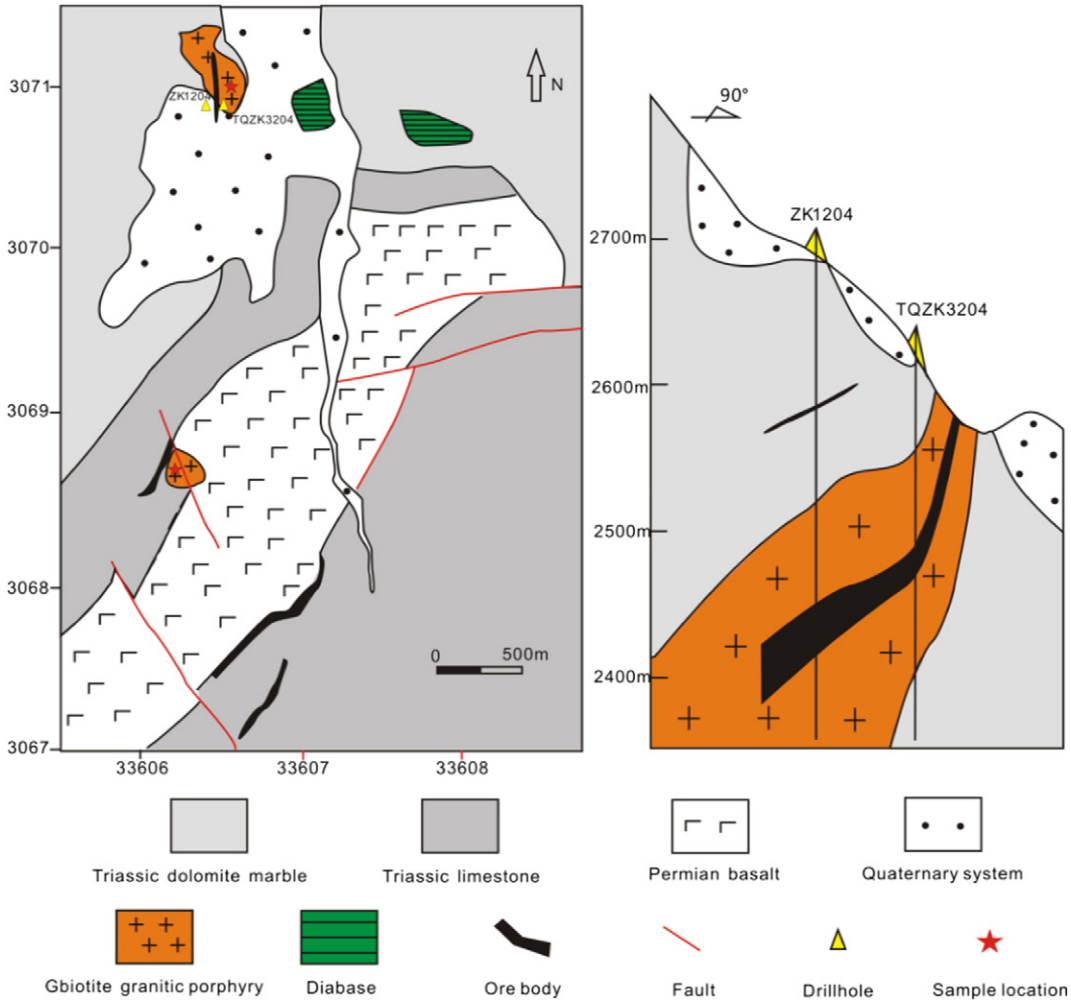

Fig. 3. Simplified geological map and cross-section of the Tongchanggou and associated porphyry Mo deposit modified after Yu et al. (2015).

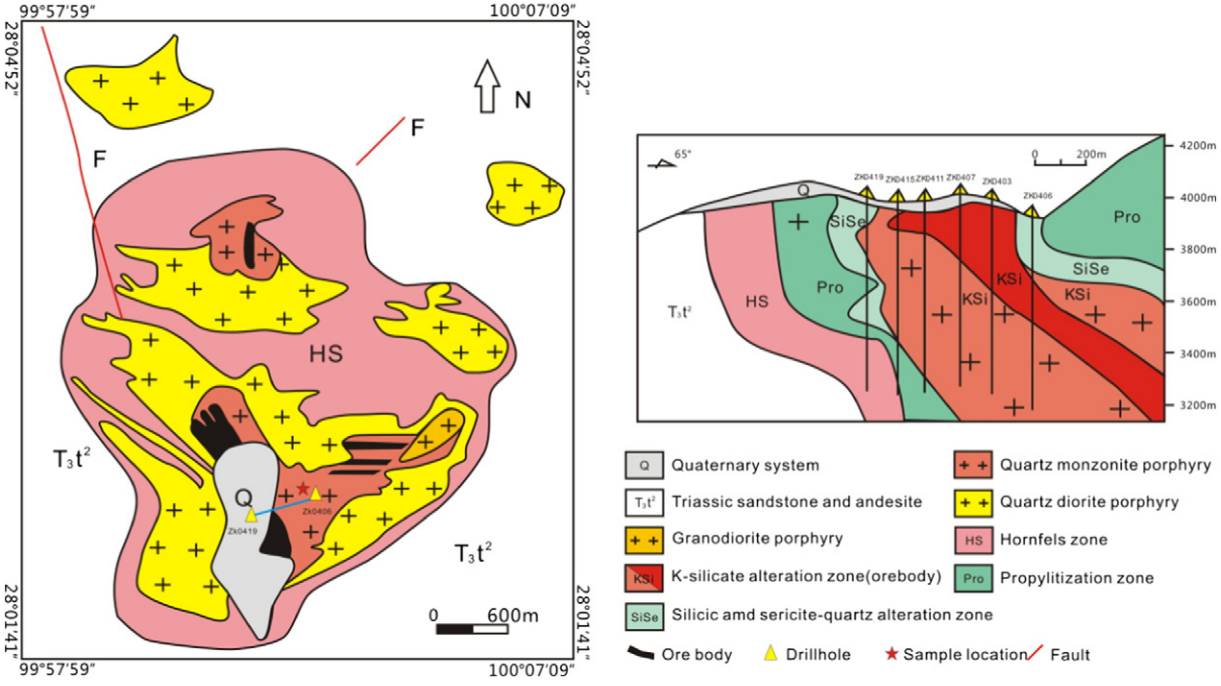

Fig. 4. Simplified geological map and cross-section of the Pulang pluton and associated porphyry Cu deposit modified after Li et al. (2011).

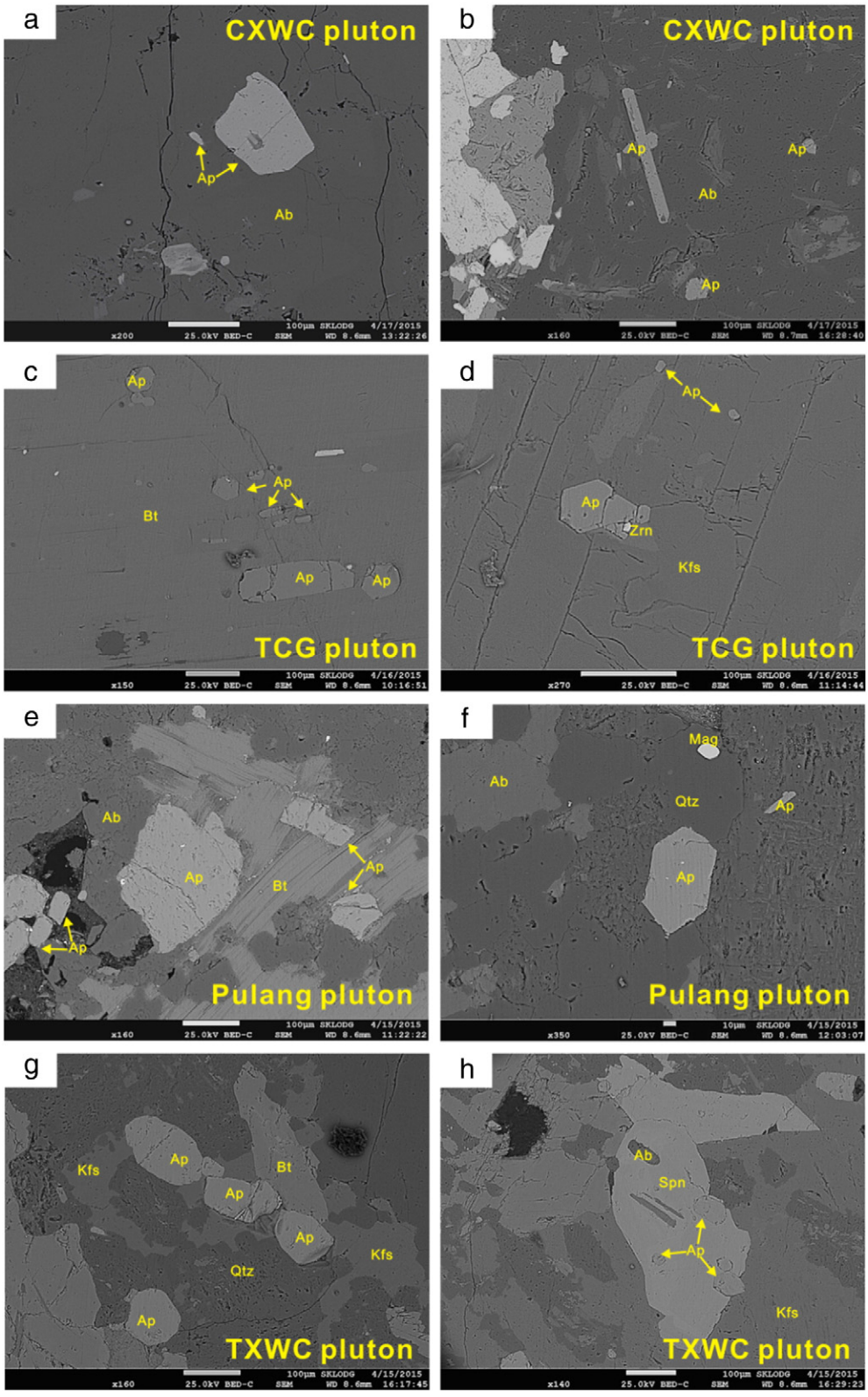

Fig. 5. Occurrences of early crystallized euhedral apatite grains from selected plutons. Ap, apatite; Ab, albite; Bt, biotite; Zrn, zircon; Kfs, K-feldspar; Mag, magnetite; Qtz, quartz; Spn, sphene.

The zircon U–Pb age of the PL pluton varies from 211 Ma to 230 Ma (Pang et al., 2014; Wang et al., 2011). Major and trace element contents of quartz monzonitic porphyry samples are listed in Appendix 1. These rocks belong to metaluminous and calc-alkaline granitoids, with Rittmann index of 2.4 and 2.8 and A/CNK of 0.94 and 0.95, and show depletions in Ba, Nb, Ta and Ti (Fig. 6f) and fractionated REE

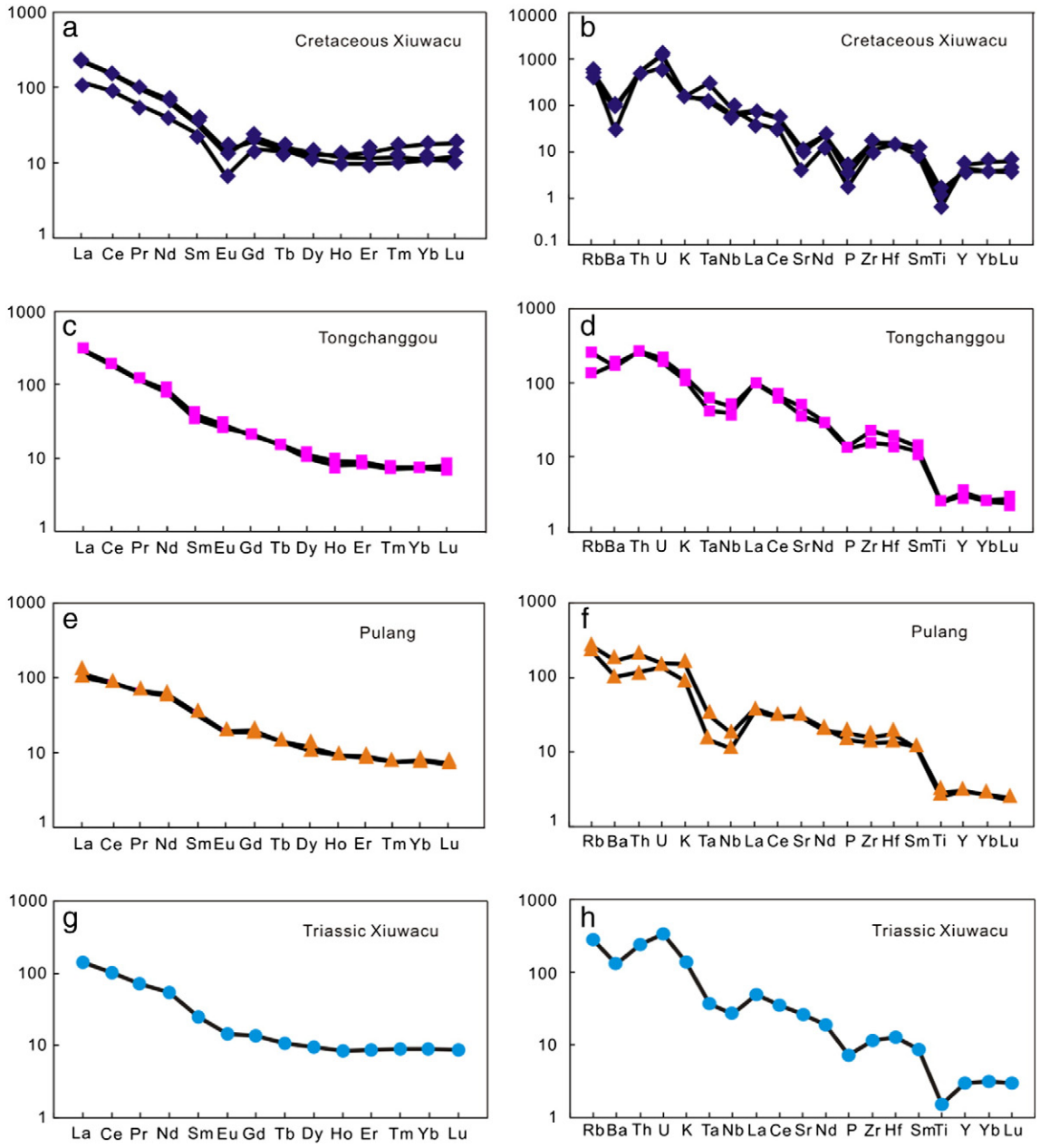

Fig. 6. Chondrite-normalised REE diagrams and primitive mantle-normalised trace element diagrams for selected plutons. Data from Appendix 1; chondrite normalizing values and primitive mantle values follow Sun and McDonough (1989).

patterns(Fig. 6e), with $(La/Yb)_N$ close to 13–15 and $Eu/Eu^* = 0.75$. Previous results show that these rocks are characterized by $(^{87}Sr/^{86}Sr)_i = 0.7065$ and $\varepsilon Nd(t) = -3$ (Li et al., 2007; Pang et al., 2014).

3.4. The Triassic Xiuwacu pluton

The TXWC pluton is located ~85 km northwest of Shangri-La city with biotite granite as main intrusive phase(Fig. 2). It is mainly composed of medium- to coarse-grained biotite. K-feldspar plagioclase, biotite and quartz are major phases. The accessory minerals include apatite, sphene and zircon. Apatite occurs as euhedral crystals surrounded by feldspar, quartz and biotite (Fig. 5g,h).

Major and trace element contents in whole rocks are listed in Appendix 1. The samples from the pluton belong to metaluminous and calc-alkaline granitoids with Rittmann index = 2.2 and A/CNK = 0.95, show depletions in Ba, Nb, Ta, P and Ti (Fig. 6h), and fractionated REE patterns (Fig. 6g) with $(La/Yb)_N$ close to 16 and $Eu/Eu^* = 0.78$.

4. Analytical methods

We select fresh rock sample without obvious alteration. The same rock sample was divided into two parts: one was used to separate apatite, and the other was prepared for whole-rock analysis.

Apatite crystals were separated from whole rock samples using standard heavy-liquid and magnetic methods, followed by hand-picking under microscope. The selected apatite grains were then mounted in epoxy, polished, and then examined using cathodoluminescence (CL) images to select good targets for in situ analysis. CL images indicate that apatite grains from the CXWC, TCG and TXWC plutons have not suffered obvious alteration. A few of the apatite grains from the PL pluton were possibly affected by alteration, we avoid such altered grains but selected fresh grains to analyze (Fig. 7).

The contents of major and minor elements in apatite were determined using a JOEL-1600 electron microprobe at the State Key Laboratory of Ore Deposit Geochemistry, Institute of Geochemistry, Chinese

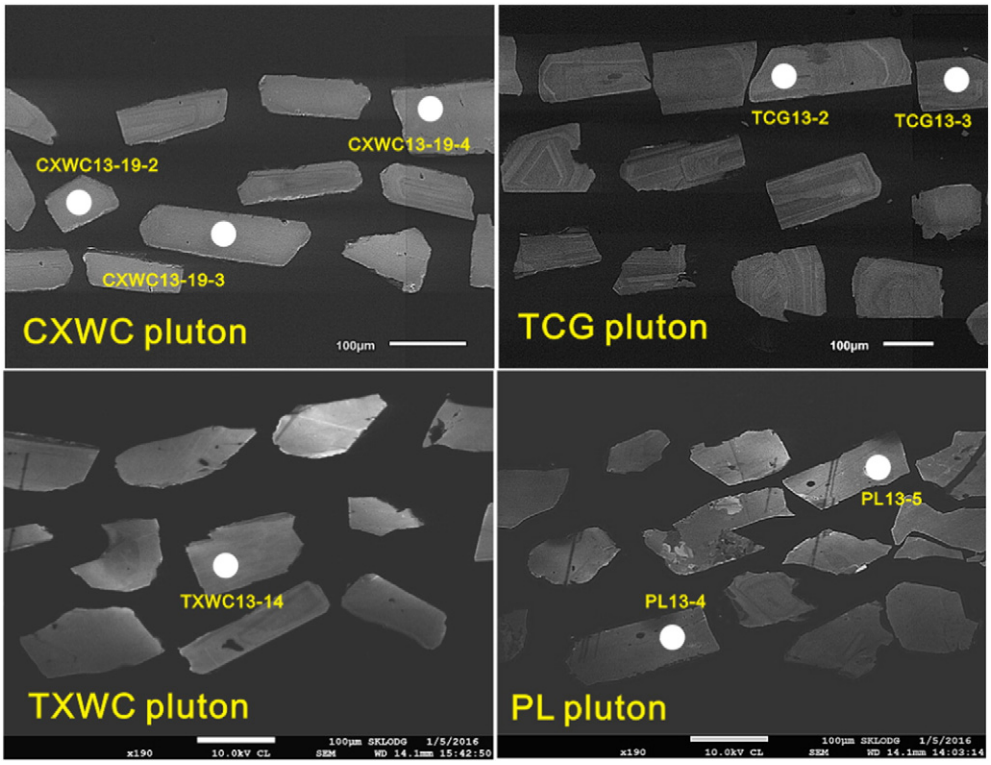

Fig. 7. CL images of representative apatites from the four plutons for in situ analysis.

Academy of Sciences in Guiyang. The analytical conditions are 25 kV accelerating voltage, 10 nA beam current and 10 μm beam diameter.

The concentrations of trace elements in apatite were measured by in situ LA-ICP-MS at the State Key Laboratory of Isotope Geochemistry, Guangzhou Institute of Geochemistry, Chinese Academy of Sciences, following the analytical procedures under the operation conditions given in Tu et al. (2011). The LA-ICP-MS system consists of an Agilent 7500a ICP-MS equipped with a Resonetics RESOLution M-50 ArF-Excimer laser gun (λ = 193 nm, 80 mJ, 10 Hz). The laser ablation spot are from 30 to 40 μm in diameter. The ablated aerosol was fed to the ICP instrument using He gas. The content of Ca was measured using ^{43}Ca and normalized using the concentration determined by electron probe analysis. The NIST610 and NIST612 standards were used for calibration. Offline data reduction was done using the ICPMSDataCal software from Liu et al. (2008). A total of 57 trace elements were analyzed. The elements of interest include Ga, Sr, Ba, Y, Zr, La, Ce, Pr, Nd, Sm, Eu, Gd, Tb, Dy, Ho, Er, Tm, Yb, Lu, Th and U. The detection limits for such elements are from 0.01–0.1 ppm, except Gd and Sm with detection limits of 0.3 ppm. Analyses of NIST610 and NIST612 as unknown samples are generally consistent with recommended values within 5% for such trace elements (see Appendix 3). The results have demonstrated high reproducibility with 0.6% to 1.8% RSD for all the trace elements of interest.

The concentrations of major elements in whole rocks associated with selected apatites were determined on fused lithium-tetraborate glass pellets using an Axios PW4400 X-ray fluorescence spectrometry at the State Key Laboratory of Ore Deposit Geochemistry, Institute of Geochemistry, Chinese Academy of Sciences, Guiyang. The analytical precision is estimated to be <5%. The concentrations of trace elements in whole rocks were analyzed using a PE DRC-e ICP-MS at the same laboratory described above. Powdered samples (50 mg) were dissolved using HF and HNO_3 acids mixture in high-pressure Teflon bombs for 2 days at about 190 °C. Rh was used to monitor signal drifting during analysis. The detailed analytical procedures are given in Qi et al. (2000). The analytical precision is estimated to be <10%.

5. Results

The ideal formula of apatite is $A_5(XO_4)_3Z$ in which the A site is occupied by Ca^{2+} and other minor or trace cations such as Sr^{2+}, Pb^{2+}, $Mg2+$, Mn^{2+}, Fe^{2+}, REE^{3+}, Eu^{2+}, Cd^{2+} and Na^{+}, the X site is occupied by P^{5+} and other minor or trace cations such as Si^{4+}, S^{6+} and C^{4+}, and the Z site is occupied by F^{-}, Cl^{-} and OH^{-}. Based on F^{-}, Cl^{-} and OH^{-} compositions, apatite can be further subdivided into fluorapatite, chlorine apatite and hydroxyapatite. Generally, minor and trace element concentrations in apatite are controlled by (1) their contents in magma, (2) their partition coefficients between apatite and melt, and (3) subsolidus element exchange reactions in the rocks. The third mechanism may obscure the magmatic information recorded by apatites. Trying to avoid such interference, We have picked out unaltered whole-rock samples and apatite crystals from the four selected intrusions, then analyzed the chemical compositions of apatite crystals by EPMA and LA-ICP-MS. The results are listed in Appendix 2.

5.1. Mn-Na-S-Si

Mn enters apatite by substituting Ca^{2+}(Pan and Fleet, 2002). The MnO contents in apatite from the PL pluton are <0.06 wt.%, with an average of 0.03 wt.%. These values are much lower than those in apatite from the CXWC pluton (0.05–0.15 wt.%, average 0.09 wt.%), the TCG pluton (0.04–0.16 wt.%, average 0.10 wt.%) and the TXWC pluton (0.01–0.08 wt.%, average 0.06 wt.%). The results show that the MnO contents in apatite and the host rocks are positively correlated. The MnO contents in the whole rock samples from the CXWC pluton (0.04–0.06 wt.%), the TCG pluton (0.06 wt.%) and the TXWC pluton (0.06 wt.%) are higher than those in the whole rock samples from the PL pluton (0.02 wt.%).

Na enters apatite by complex substitutions such as $Na^{+} + S^{6+} = Ca^{2+} + P^{5+}$, $2Na^{+} = Ca^{2+} + [V]$, and $REE^{3+} + Na^{+} = 2Ca^{2+}$. (RØnsbo, 1989; Sha and Chappell, 1999). The Na_2O contents in apatite

crystals from the selected plutons are close to or below the detection limit.

S enters apatite by complex substitutions such as $Na^{+} + S^{6+} = Ca^{2+} + P^{5+}$ and $S^{6+} + Si^{4+} = 2P^{5+}$(Sha and Chappell, 1999). The SO_3 contents in apatite from the CXWC pluton are mostly below the detection limit and much lower than those in apatite from the TCG pluton (0.08–0.22 wt.%, average 0.13 wt.%), the PL pluton (<0.38 wt.%, average 0.13 wt.%) and the TXWC pluton (0.08–0.18 wt.%, average 0.12 wt.%).

Si enters apatite by complex substitutions such as $S^{6+} + Si^{4+} = 2P^{5+}$ and $REE^{3+} + Si^{4+} = Ca^{2+} + P^{5+}$(Pan and Fleet, 2002; RØnsbo, 1989; Sha and Chappell, 1999).The SiO_2 contents in apatite from the selected plutons are similar (CXWC, 0.10–0.52 wt.%, average 0.25 wt.%; TCG, <0.19 wt.%, average 0.12 wt.%; PL, 0.08–0.35 wt.%, average 0.16 wt.%; TXWC, 0.15–0.39 wt.%, average 0.27 wt.%). The results show no absolute correlation between apatite and whole rock Si contents. The CXWC pluton, which has the highest SiO_2 contents in whole rocks among the four selected plutons, does not show the highest SiO_2 contents in apatite.

5.2. Halogens

Cl^{-} is present in apatite by substituting F^{-} or OH^{-}(Pan and Fleet, 2002). Our results show a relatively negative correlation between F and Cl in apatite from the four selected plutons (Fig. 8). The negative correlation between F and Cl is influenced by the substitution of H_2O for F and Cl. The results also show that all of the apatite crystals are rich in F (mostly ≥2.8 wt.%) and poor in Cl (mostly ≤0.4 wt.%). The F contents in apatite from the CXWC pluton (3.27–4.89 wt.%, average 3.97 wt.%) are slightly higher than those of apatite from the TCG pluton (2.60–4.80 wt.%, average 3.00 wt.%), from the PL pluton (2.67–3.51 wt.%, average 2.98 wt.%) and from the TXWC pluton (2.93–3.77 wt.%, average 3.26 wt.%). The Cl contents of apatite from the CXWC pluton (some analyses below the detection limit) are generally lower than those of apatite from the other three plutons (TXWC, 0.04–0.26 wt.%, average 0.10 wt.%; TCG, 0.08–0.34 wt.% average 0.17 wt.%; PL, 0.03–0.43 wt.%, average 0.18 wt.%).

5.3. Sr-Zr-Th-Ga-REE

Sr is present in apatite by substituting Ca^{2+}(Pan and Fleet, 2002). The results show the highest Sr contents in apatite from the TCG pluton (202–1014 ppm, average 745 ppm), intermediate Sr contents in apatite from the PL pluton (285–1200 ppm, average 626 ppm) and the TXWC pluton (346–413 ppm, average 384 ppm), and the lowest Sr contents in apatite from the CXWC pluton (110–495 ppm, average 292 ppm). Generally, the Sr contents in the apatite crystals are positively correlated with those in the whole rocks.

Zr enters apatite by complex substitutions such as $Zr^{4+} + Si^{4+} = REE^{3+} + P^{5+}$ and $Ca^{2+} + Zr^{4+} = 2REE^{3+}$ (Casillas et al., 1995). The CXWC pluton does not have higher Zr contents in whole rocks but has higher Zr contents in apatite (<11 ppm, average 3 ppm) as compared to the other three plutons (TCG, <3 ppm, average 0.6 ppm; PL, <1.4 ppm, average 0.9 ppm; TXWC, <0.9 ppm, average 0.5 ppm).

Th enters apatite by complex substitutions such as $Th^{4+} = 2Ca^{2+}$, $Th^{4+} + Si^{4+} = REE^{3+} + P^{5+}$ and $Ca^{2+} + Th^{4+} = 2REE^{3+}$ (Casillas et al., 1995). Apatite crystals from the CXWC pluton and the TCG pluton have less Th contents (CXWC, 18–82 ppm, average 35 ppm; TCG,16–44 ppm, average 31 ppm) than those from the PL pluton and the TXWC pluton (PL, 45–87 ppm, average 68 ppm; TXWC, 25–84 ppm average 56 ppm), which is the reverse of Th contents in whole rocks.

Ga enters apatite by substituting Ca^{2+}. The highest Ga content (14–44 ppm, average 22 ppm) is detected in the apatite from the CXWC pluton. Apatite from the PL and TXWC plutons has moderate Ga content (PL:12–21 ppm, average17 ppm; TXWC: 11–19 ppm, average 15 ppm). Apatite from the TCG pluton has lowest Ga content (7–15 ppm, average 10 ppm). Such order is different from that of the whole rock Ga that shows nearly similar content (17–20 ppm). It thus means the different Ga content in apatite is not entirely controlled by the magma composition.

Individual REE enters apatite by complex substitutions such as $2REE^{3+} + [V] = 3Ca^{2+}$, $REE^{3+} + Na^{+} = 2Ca^{2+}$ and $REE^{3+} + Si^{4+} = Ca^{2+} + P^{5+}$(Pan and Fleet, 2002; RØnsbo, 1989; Sha and Chappell, 1999). The results show the highest total REE contents in apatite from the CXWC pluton (4582–14,373 ppm, average 7239 ppm), intermediate total REE contents in apatite from the PL pluton (4066–7290 ppm, average 6008 ppm) and the TXWC pluton (3456–6303 ppm, average 4826 ppm), and the lowest total REE contents in apatite from the TCG pluton (2424–4115 ppm, average 3334 ppm). The total REE contents in apatite are not systematically correlated with whole rock REE concentrations.

The chondrite-normalised REE patterns of apatite from the four selected plutons (Fig. 9) all show light REE enrichments relative to heavy REE and variable degrees of negative Eu anomaly. The degrees of light REE enrichments in apatite from the four selected plutons, in descending order, are PL, TCG, TXWC and CXWC. The degrees of Eu anomaly in apatite from the plutons, in descending order, are TCG, PL, TXWC and CXWC.

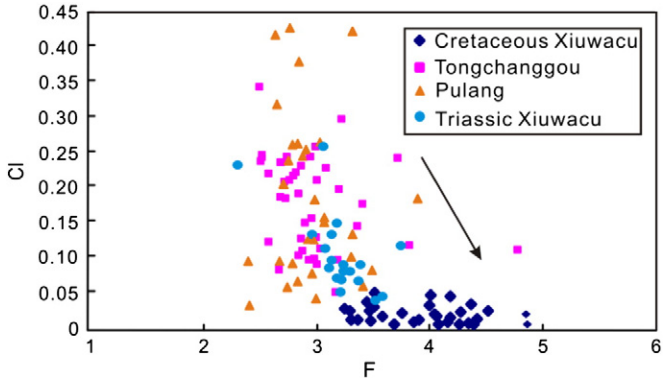

Fig. 8. Plots of F (wt.%) vs Cl (wt.%) in apatites from four selected plutons.

6. Discussion

6.1. Controls on REE characteristics in apatite

As shown in Fig. 5, apatite from the four selected granite plutons commonly occurs as euhedral crystals enclosed in silicate minerals. This textural relationship combined with high apatite saturation temperatures of more than 850 °C(Appendix 1) indicates that apatite in these rocks is one of the early crystal phases to appear on liquidus. Thus, the abundances of trace elements such as REE in apatite are mainly controlled by their concentrations in the parental melt and their partition coefficients between apatite and melt.

It is common to use whole-rock compositions of granitoids to represent the compositions of their parental melt, because crystal fractionation in felsic magma is generally insignificant due to the high magma viscosity. Experiments showed that the apatite/melt partition coefficients for middle REE such as Sm are higher than those for light REE such as La and heavy REE such as Yb (Fujimaki, 1986; Watson and Green, 1981). This explains why apatite crystals from granitoids commonly have lower $(La/Sm)_N$ and $(Yb/Sm)_N$ than host rocks. This relationship is also present in three out of the four granite plutons we have studied. The PL pluton is an exception. Most apatite crystals from this pluton have higher $(La/Sm)_N$ ratios (2.8–8.7) than that of the host rock (3–3.5).

There are two possible explanations for the unusual relationship in REE compositions between apatite and whole rock in the PL pluton. Firstly, the experimental results from Watson and Green (1981) and

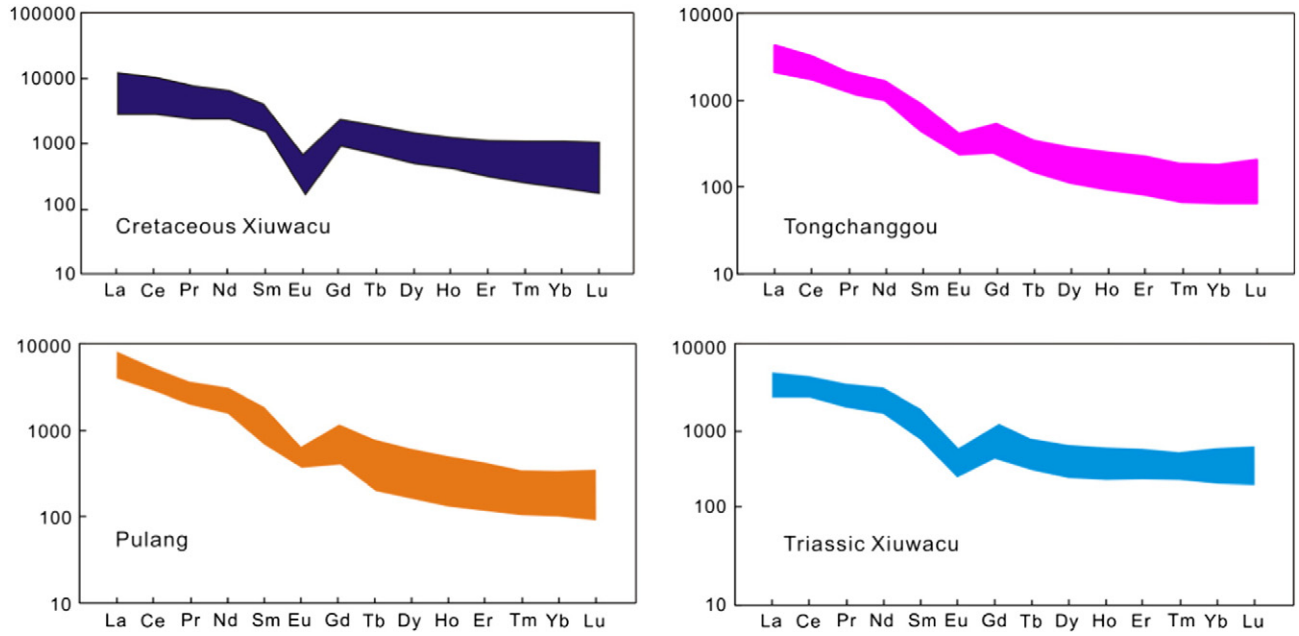

Fig. 9. Chondrite-normalised REE distribution patterns for apatites from the four selected plutons. Data from Appendix 2; chondrite normalizing values and primitive mantle values follow Sun and McDonough (1989).

Fujimaki (1986) may not be suitable for the PL magmatic system due to different conditions between nature and the experiments. However, many recent experiments that were conducted under these conditions are significantly different from those of Watson and Green (1981) and Fujimaki (1986) (e.g. Ayers and Watson, 1993; Macdonald et al., 2008; Prowatke and Klemme, 2006), which also show that middle REE are more compatible in apatite than both light REE and heavy REE. Thus, this explanation can be ruled out.

The second possibility is that the whole-rock REE could not represent the REE in the melt when apatite crystallized owing to the earlier saturation of other REE-rich minerals. It is worthwhile to note that euhedral sphenes occur in the PL pluton. The experimental results from Green and Pearson (1986) have indicated middle REE such as Sm is more compatible than light REE such as La in sphene. Thus, early saturation of shpene depleted Sm relative to La in residual melt. Apatites crystallized from such residual melt inherited higher $(La/Sm)_N$ ratio than that calculated through whole-rock REE.

6.2. Apatite Ga content and δEu as indicators of magma oxidation state

The abundances of Mn, Eu, S and Ce in apatite may be used to evaluate the oxidation state of magma (e.g. Cao et al., 2012; Drake, 1975; Imai, 2002, 2004; Peng et al., 1997; Sha, 1998; Sha and Chappell, 1999; Streck and Dilles, 1998). More oxidized magma increase Mn^{4+}, Eu^{3+} Ce^{4+} at the expense of Mn^{2+}, Eu^{2+}, Ce^{3+} in the melt. Mn^{2+}, Eu^{3+} and Ce^{3+} are favored by apatite, because they can substitute Ca^{2+} in apatite (Belousova et al., 2002; Sha and Chappell, 1999). As a result, apatite crystallizing from more oxidized magma will have higher Eu but lower Mn and Ce than more reduced magma if the concentrations of these elements in the magmas are equal.

However, the variation of a single element in apatite cannot be used to determine the change in magma oxidation state because it may be controlled by other factors. For example, The concentration of Mn in magma may vary during crystallization (Belousova et al., 2002; Chu et al., 2009) and the content of Eu in magma may decrease due to feldspar fractionation (Ballard et al., 2002; Bi et al., 2002; Buick et al., 2007). Consequently, The variations of two multi-variance elements such as Eu and Ce, which have opposite partitioning behavior into apatite in response to change in oxidation state, are more useful. As shown in Fig. 10b, δEu and δCe in apatite from the CXWC pluton are negatively correlated, indicating that these proxies are intensely affected by oxidation state in this magma system. In contrast, apatite crystals from the TCG, PL and TXWC plutons don't display such correlation, indicating that oxidation state is not the only major controlling factors for the abundances of these elements in apatite in these magmatic systems. Such factors could also explain the noncorrelation between MnO and δEu in apatite(Fig. 10c).

Our results show that the concentrations of Ga vary only slightly in host rocks but dramatically in apatite crystals, which implies the melt composition is not the controlling factor of different Ga content in apatite. δEu as a valid oxidation state proxy for granitic has been successfully applied (e.g. Cao et al., 2012). The negative correlation between apatite Ga and δEu (Fig. 10a), further indicates Ga variation is more likely to result from different oxidation states in the selected plutons. Ga has two common valence states, +2 and +3. Ga^{2+} is preferred by apatite because of the same valence state with Ca^{2+}. Thus, lower oxidation state increases Ga in apatite if other controlling factors such as Ga contents in magma remain the same. The order of Ga concentrations in apatite, in decreasing order, is the CXWC pluton (14–44 ppm, average 22 ppm), the PL pluton (12–21 ppm, average17 ppm), the TXWC pluton (11–19 ppm, average 15 ppm) and the TCG pluton (7–15 ppm, average 10 ppm). This, together with a negative correlation between Ga and δEu for all of the samples (Fig. 10a), indicates that the parental magmas became more reduced in this order: TCG, TXWC, PL and CXWC. This result is consistent with the calculated Fe^{2+}/Fe^{3+} ratios in whole rocks (TCG, 1.8 and 1.5; TXWC, 2.3; PL, 3.5 and 2.6; CXWC, 4.7–9.7).

6.3. Apatite Sr/Y and δEu as proxies for adakite-like rocks

Based on the chemical classification of Defiant and Drummond (1990) and Drummond and Defant (1990), the PL, TCG and TXWC plutons are adakite-like, whereas the CXWC pluton is not. Adakitic magma is characterized by higher Sr, lower Y and Yb, and lack of negative Eu anomaly than other types of felsic magma, because adakitic magma is generated at greater depth in the crust where feldspar, which is a sink for both Sr and Eu, is unstable. Partial melting of the same source at shallower depth where feldspar is a residual phase will produce magma containing higher Y and Yb, and lower Sr and Eu (Peacock et al., 1994; Rapp and Watson, 1995; Rapp et al., 1999, 2002; Sen and Dunn, 1994, 1995).

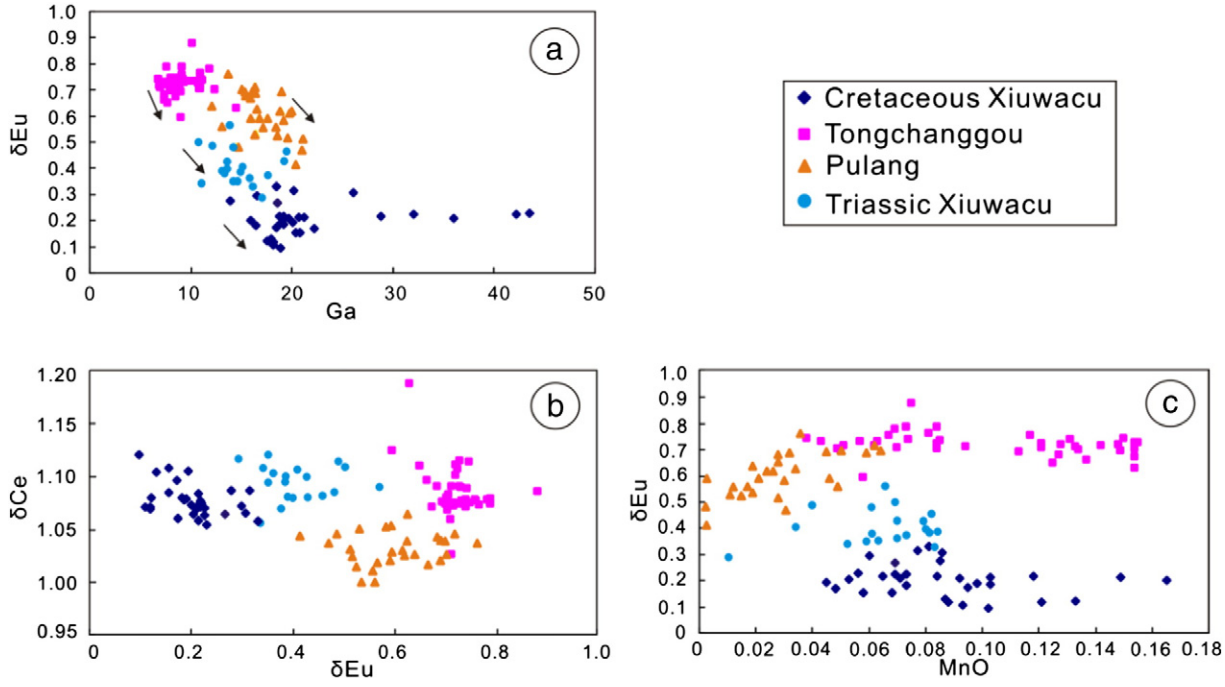

Fig. 10. Plots of (a) δEu vs Ga contents (ppm), (b) δEu vs δCe and (c) δEu vs MnO contents (wt.%) in apatites from the four selected plutons.

As shown in Fig. 11, a positive correlation between Sr/Y and δEu in apatite exists for two adakite-like plutons plus a non-adakite pluton. Overall, apatite crystals from the adakite-like plutons have higher Sr/Y and δEu than apatite crystals from the non-adakite pluton. This matches the whole rock compositional variations and indicates that Sr/Y and δEu in apatite can be used to identify adakite-like rocks, especially for those highly altered or weathered rocks that do not preserve the original Sr/Y ratios. This finding is significant, because Sr and Eu in felsic rocks are mainly hosted in feldspars that are susceptible to alteration. In contrast, apatite is not susceptible to alteration compared to feldspar. However, it would be very carefully to use this method when apatite is not the early phase. Because apatite crystallized from the evolving magma undergoing massive fractional crystallization may not reflect real Sr/Y ratio and δEu value of the parental magma.

6.4. Apatite REE ratios and Sr contents as indicators of fractionation pathway

The change of trace element composition in apatite may reflect magma compositional variation as the result of crystallization of other minerals. For example, crystallization of feldspars, the main host of Sr in felsic magma, will decrease Sr in the residual melt. During this process, apatite crystallizing late will have lower Sr content than that crystallizing earlier. Thus, the variation of Sr contents in apatite from a suite of rocks may be used to track magma evolution by this process. REE-rich mineral crystallization from magma will fractionate these elements in the magma and hence the apatite crystallizing from such magma as well. Thus, the combination of REE ratios such as $(La/Sm)_N$ $(La/Yb)_N$,$(Sm/Yb)_N$ and Sr content in apatite may be used to evaluate the crystallization history of a pluton.

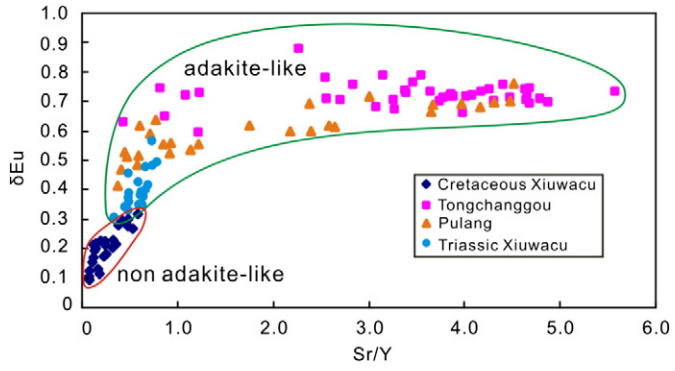

Fig. 11. Plots of δEu vs Sr/Y in apatites from the four selected plutons.

As shown in Fig. 12, all of the analyses for apatite from the four selected granite plutons together show that the$(La/Sm)_N$ $(La/Yb)_N$, and $(Sm/Yb)_N$ ratios are positively correlated with Sr contents. Such correlation presenting in a single pluton such as the CXWC, TCG and PL plutons, indicate that early crystallization of feldspars played a significant role in magma differentiation. Allanite involved magmatic fractionation resulting in the decreasing ratios of $(La/Sm)_N$, $(La/Yb)_N$, and $(Sm/Yb)_N$ in apatite from the first two plutons. The TXWC pluton show the rather constant contents of Sr in apatite. This means that feldspars are not important early phases. However, The rapid decrease in $(La/Sm)_N$, $(La/Yb)_N$ and $(Sm/Yb)_N$ ratios with the decreased or constant Sr content in apatite from the PL and TXWC plutons are not likely to result from the fractionation of other LREE-rich minerals, because no allanite or monazite have been found in samples. Instead of it, the exsolution of bearing-Cl hydrotherm is a possible cause for the rapid decrease in $(La/Sm)_N$, $(La/Yb)_N$ and $(Sm/Yb)_N$ ratios. Previous experiments (e.g. Flynn and Burnham, 1978; Keppler, 1996) have indicated the exsolution of bearing-Cl hydrotherm could take away more LREE than MREE and HREE from melt. Apatites crystallized from such melt inherit decreasing $(La/Sm)_N$, $(La/Yb)_N$ and $(Sm/Yb)_N$. This supposition could be supported by the negative correlations of F/Cl and $(La/Yb)_N$ in apatites (Fig. 13).

6.5. Apatite halogen composition as a record of magmatic volatiles

The Cl/F ratios in apatite from the four granite plutons studied by us, in decreasing order, are PL (0.01–0.16, average 0.06), TCG (0.01–0.14, average 0.06), TXWC (0.01–0.08, average 0.03) and CXWC (<0.01, average < 0.01). The results show that apatite crystals from the plutons that host the porphyry-type Cu deposit (PL) or Mo deposit (TCG) have higher Cl/F ratios than those from the pluton that hosts vein-type Mo deposit (CXWC) and unmineralized pluton (TXWC). It is widely known that apatite is not vulnerable to subsolidus halogen exchange

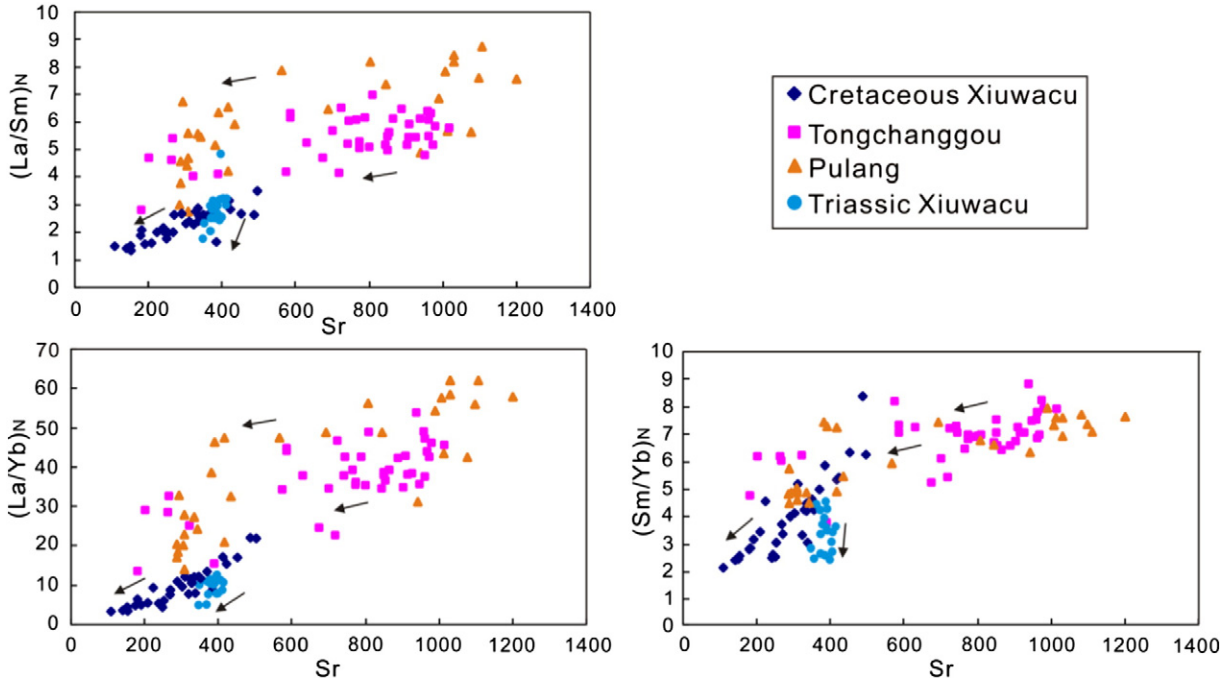

Fig. 12. Plots of $(La/Sm)_N$, $(La/Yb)_N$ and $(Sm/Yb)_N$ vs Sr contents (ppm) in apatites from the four selected plutons.

(Piccoli and Candela, 1994; Roegge et al., 1974; Tacker and Stormer, 1989). Cl/F ratio in fresh apatite, to a great extent, reflects this ratio in the systems they crystallized from. Thus, our results provide indirect evidence for different Cl/F ratios in the parental magmas of the granite plutons with different types of mineralization.

Among the three mineralized plutons we have studied, the inferred Cl/F ratio in the parental magma of the CXWC pluton is the lowest. The reasons for this difference are not clear but one possibility is source control. The parental magma of the CXWC pluton was generated by anataxis of continental crust (Wang et al., 2014b), a source with extremely low Cl/F ratio. In contrast, slab-derived fluids, which have higher Cl/F ratios, were either directly or indirectly involved in the generation of the parental magmas for the other three plutons (Meng, 2014; Zeng et al., 2006). Alternatively, the difference may have resulted from variable degrees of degassing which fractionated Cl and F (e.g. Boudreau and Kruger, 1990; Candela, 1986; Warner et al., 1998). However, constant Cl/F ratios equal to 0 in apatites from the CXWC pluton display no systematical changes during degassing. Thus, even though we cannot entirely rule out this possibility, by comparison, we favor the former explanation.

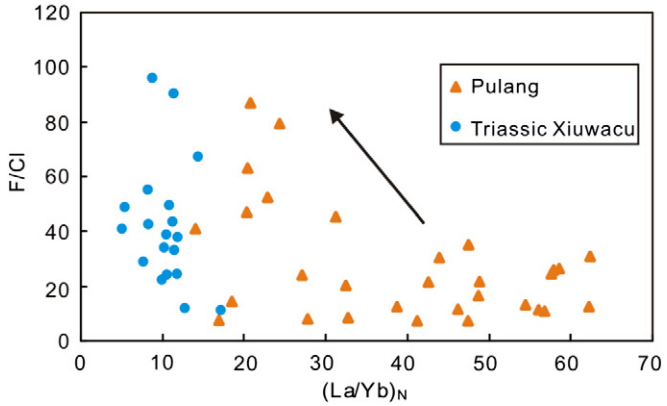

Fig. 13. Plots of Cl/F vs $(La/Yb)_N$ in apatites from the PL pluton and TXWC plutons.

6.6. Apatite as an indicator of mineralization potential

As described above, apatite trace element and halogen compositions generally reflect magma conditions. This, together with the fact that apatite is less susceptible to alteration, which is a key feature of mineralized granite plutons, than other minerals such as feldspar, mica and hornblende in the plutons, makes apatite a useful tool for evaluating the mineralization potential of granite plutons in mineral exploration.

Our results reveal that apatite crystals from the adakite-like plutons that host porphyry-type Cu or Mo deposits have higher Sr/Y and δEu than those from the pluton that host vein-type Mo deposits. The host rocks of the vein-type Mo deposit are characterized by significantly lower Cl/F in apatite than those of porphyry-type deposits. Among the three adakite-like plutons, the unmineralized pluton (TXWC) is characterized by the lowest Cl/F in apatite but moderate oxidation state. Between the porphyry-type Cu and Mo deposits, the parental magma of the latter, as indicated by apatite composition, is more oxidized than that of the former. The significance of the finding is yet to be determined by study of more deposits.

The apatite data show that the parental magmas of the porphyry-type ore systems were more oxidized than that of the vein-type Mo deposit. This is expected because high oxidation state prevents early crystallization of Fe-sulphide that remove Cu and Mo from magma before the ore-forming fluids are exsolved from the magma (Candela and Bouton, 1990; Hedenqulst and Lowenstern, 1994; Sillitoet, 2010; Tacker and Candela, 1987). Vein-type Mo deposit is related to more F-rich fluids in which Mo can be bounded with S to form ore minerals under reduced conditions (Liu et al., 2013; Xu and Zhang, 2012) that may prevent the formation of large deposits (like PL and TCG) in CXWC.

7. Conclusions

Most significant findings from this study are listed below.

(1) Sr, REE and halogens in apatite can be used to track the abundances and changes of these elements in the parental magmas and crystallization history of the magmas.
(2) Ga contents and its negative correlation with δEu in apatite can indicate oxidation states of magmas.

(3) The combination of Sr/Y ratios and δEu in apatite is a useful tool to identify adakite-like plutons that have lost initial Sr/Y ratios in whole rocks due to weathering and hydrothermal alteration.
(4) The parental magmas for two adakite-like plutons containing porphyry-type Cu and Mo deposits are more oxidized than that for a different type of pluton containing vein-type Mo deposits.
(5) Apatite crystals from the host rocks of a vein-type Mo deposit are characterized by much lower Cl/F ratios than those from the host rocks of porphyry-type Cu and Mo deposits. Apatite crystals from a unmineralized adakite-like pluton are characterized by lower Cl/F ratios than those from Cu- and Mo-mineralized adakite-like plutons.

Acknowledgements

This study was jointly supported by the Key Natural Science Foundation of China (41130423), the 12th Five-Year Plan Project of the State Key Laboratory of Ore Deposit Geochemistry, Chinese Academy of Sciences (SKLODG-ZY125-03) and the CAS/SAFEA International Partnership Program for Creative Research Teams—(Intraplate Mineralization Research Team; KZZD-EW-TZ-20). We thank Ms. Chong-Yin Li for the apatite trace elements analysis by LA-ICP-MS; Ms. Wen-Qin Zheng for the apatite major and minor elements analysis by EPMA; Prof. You-Wei Chen for the apatite BSE and CL imaging; Ms. Jing Hu and Ms. Guang-Ping Bao for the whole-rock analysis by XRF and ICP-MS. Dr. Lei-Luo Xu is thanked for discussion with him giving us lots of ideas. Prof. Sun.-Lin Chung and two anonymous reviewers are thanked for their constructive and detailed reviews of this manuscript.

Appendix A. Supplementary data

Supplementary data to this article can be found online at http://dx.doi.org/10.1016/j.lithos.2016.03.010.

References

Ayers, J.C., Watson, E.B., 1991. Solubility of apatite, monazite, zircon, and rutile in supercritical aqueous fluids with implications for subduction zone geochemistry. Philosophical Transactions of the Royal Society A335, 365–375.
Ayers, J.C., Watson, E.B., 1993. Apatite/fluid partitioning of rare earth elements and strontium: experimental results at 1.0 GPa and 1000 °C and application to models of fluid–rock interaction. Chemical Geology 110, 299–314.
Ballard, J.R., Palin, J.M., Campbell, I.H., 2002. Relative oxidation states of magmas inferred from Ce(IV)/Ce(III) in zircon: application to porphyry copper deposits of Northern Chile. Contributions to Mineralogy and Petrology 144, 347–364.
Belousova, E.A., Walters, S., Griffin, W.L., O'Reilly, S.Y., 2001. Trace-element signatures of apatites in granitoids from the Mt. Isa Inlier, northwestern Queensland. Australian Journal of Earth Sciences 48, 603–619.
Belousova, E.A., Griffin, W.L., O'Reilly, S.Y., Fisher, N.I., 2002. Apatite as an indicator mineral for mineral exploration: trace-element composition and their relationship to host rock type. Journal of Geochemical Exploration 76, 45–69.
Bi, X.W., Cornell, D.H., Hu, R.Z., 2002. REE composition of primary and altered feldspar from the mineralized alteration zone of alkali-rich intrusive rocks, Western Yunnan Province, China. Ore Geology Reviews 19, 69–78.
Boudreau, A.E., 1993. Chlorine as an exploration guide for the platinum-group elements in layered intrusions. Journal of Geochemical Exploration 48, 21–37.
Boudreau, A.E., Kruger, F.J., 1990. Variation in the composition of apatite through the Merensky cyclic unit in the Western Bushveld Complex. Economic Geology 85, 737–745.
Boudreau, A.E., McCallum, I.S., 1989. Investigations of the Stillwater Complex: part V. Apatites as indicators of evolving fluid composition. Contributions to Mineralogy and Petrology 102, 138–153.
Boyce, J.W., Hervig, R.L., 2009. Apatite as a monitor of late-stage magmatic processes at Volca'n Irazu´, Costa Rica. Contributions to Mineralogy and Petrology 157, 135–145.
Boyce, J.W., Liu, Y., Rossman, G.R., Guan, Y.B., Eiler, J.M., Stolper, E.M., Taylor, L.A., 2010. Lunar apatite with terrestrial volatile abundances. Nature 466, 466–470.
Buick, I.S., Hermann, J., Maas, R., Gibson, R.L., 2007. The timing of subsolidus hydrothermal alteration in the central zone, Limpopo Belt (South Africa): constraints from titanite U–Pb geochronology and REE partitioning. Lithos 98, 97–117.
Candela, P.A., 1986. Toward a thermodynamic model for the halogens in magmatic systems: an application to melt-vapor-apatite equilibria. Chemical Geology 57, 289–301.
Candela, P.A., Bouton, S.L., 1990. The influence of oxygen fugacity on tungsten and molybdenum partitioning between silicate melts and ilmenite. Economic Geology 85, 633–640.
Cao, M.J., Li, G.M., Qin, K.Z., Seitmuratova, E.Y., Liu, Y.S., 2012. Major and trace element characteristics of apatites in granitoids from Central Kazakhstan: implications for petrogenesis and mineralization. Resource Geology 62, 63–83.
Casillas, R., Nagy, G., PantÓ, G., Brändle, J., FÓrizs, I., 1995. Occurrence of Th, U, Y, Zr, and REE-bearing accessory minerals in late-Variscan granitic rocks from the Sierra de Guadarrama (Spain). European Journal of Mineralogy 7, 989–1006.
Cawthorn, R.G., 1994. Formation of chlor- and fluor-apatite in layered intrusions. Mineralogical Magazine 38, 299–306.
Chew, D.M., Sylvester, P.J., Tubrett, M.N., 2011. U–Pb and Th–Pb dating of apatite by LA-ICP-MS. Chemical Geology 280, 200–216.
Chu, M.F., Wang, K.L., Griffin, W.L., Chung, S.L., O'Reilly, S.Y., Norman, J.P., Ilzuka, Y., 2009. Apatite composition: tracing petrogenetic processes in Transhimalayan granitoids. Journal of Petrology 50, 1829–1855.
Corbett, G.J., Leach, T.M., 1998. Southwest Pacific Rim gold–copper systems: structure, alteration and mineralisation. Economic Geology, Special Publication 6, 238.
Corfu, F., Stone, D., 1998. The significance of titanite and apatite U–Pb ages: constraints for the post-magmatic thermal-hydrothermal evolution of a batholitic complex, Berens River area, Northwestern Superior Province, Canada. Geochimica et Cosmochimica Acta 62, 2979–2995.
Creaser, R.A., Gray, C.M., 1992. Preserved initial $^{87}Sr/^{86}Sr$ in apatite from altered felsic igneous rocks: a case study from Middle Proterozoic of South Australia. Geochimica et Cosmochimica Acta 56, 2789–2795.
Defiant, M.J., Drummond, M.S., 1990. Derivation of some modern arc magmas by melting of young subducted lithosphere. Nature 347, 662–665.
Drake, M.J., 1975. Oxidation state of europium as an indicator of oxygen fugacity. Geochimica et Cosmochimica Acta 39, 55–64.
Drummond, M.S., Defant, M.J., 1990. A mode for trondhjemite-tonalite-dacite genesis and crustal growth via slab melting: Archean to Modern comparisons. Journal of Geochemical Exploration 95, 21503–21521.
Ekstrom, T.K., 1972. The distribution of fluorine among some coexisting minerals. Contributions to Mineralogy and Petrology 34, 192–200.
Elkins-Tanton, L.T., Grove, T.L., 2011. Water (hydrogen) in the lunar mantle: results from petrology and magma ocean modeling. Earth and Planetary Science Letters 307, 173–179.
Flynn, R.T., Burnham, C.W., 1978. An experiment determination of rare earth partition coefficients between chlorine containing vapor and silicate melts. Geochimica et Cosmochimica Acta 42, 685–701.
Fujimaki, H., 1986. Partition coefficients of Hf, Zr, and REE between zircon, apatite and liquid. Contributions to Mineralogy and Petrology 94, 42–45.
Gaweda, A., Szopa, K., Chew, D.M., 2014. LA-ICP-MS U–Pb dating and REE patterns of apatite from the Tatra Mountains, Poland as a monitor of the regional tectonomagmatic activity. Geochronometria 41, 306–314.
Green, T.H., Pearson, N.J., 1986. Rare-earth element partitioning between sphene and coexisting silicate liquid at high pressure and temperature. Chemical Geology 55, 105–119.
Harrison, T.M., Watson, E.B., 1984. The behavior of apatite during crustal anatexis: equilibrium and kinetic consideration. Geochimica et Cosmochimica Acta 48, 1467–1477.
Hedenqulst, J.W., Lowenstern, J.B., 1994. The role of magmas in the formation of hydrothermal ore deposits. Nature 370, 519–527.
Henerson, P., 1980. Rare earth element partition between sphene, apatite and other coexisting minerals at the Kangerdlugssuag Intrusion, East Greenland. Contributions to Mineralogy and Petrology 72, 81–85.
Hou, Z.Q., 1993. Tectono-magmatic evolution of the Yidun Island-arc and geodynamic setting of Kuroko-type sulfide deposits in Sanjiang region, China. Resource Geology (Special Issue) 17, 336–357.
Imai, A., 2002. Metallogenesis of porphyry Cu deposits of the western Luzon arc, Philippines: K-Ar ages, SO_3 contents of microphenocrystic apatite and significance of intrusive rocks. Resource Geology 52, 147–161.
Imai, A., 2004. Variation of Cl and SO_3 contents of microphenocrystic apatite in intermediate to silicic igneous rocks of Cenozoic Japanese island arcs: implications for porphyry Cu metallogenesis in the Western Pacific Island arcs. Resource Geology 54, 357–372.
Jahnke, R.A., 1984. The synthesis and solubility of carbonate fluorapatite. American Journal of Science 284, 58–78.
Keppler, H., 1996. Constraints from partitioning experiments on the composition of subduction zone fluid. Nature 380, 237–240.
Leng, C.B., Zhang, X.X., Wang, S.X., Qin, C.J., Gao, T.Z., 2007. Geochemical characteristics of porphyry copper deposits in the Zhongdian area, Yunnan as exemplified by the Xuejiping and Pulang porphyry copper deposits. Acta Mineralogica Sinica 27, 414–422.
Leng, C.B., Huang, Q.Y., Zhang, X.C., Wang, S.X., Zhong, H., Hu, R.Z., Bi, X.W., Zhu, J.J., Wang, X.S., 2014. Petrogenesis of the Late Triassic volcanic rocks in the Southern Yidun arc, SW China: constraints from the geochronology, geochemistry, and Sr-Nd-Pb-Hf isotopes. Lithos 190–191, 363–382.
Li, W.C., 2007. The Tectonic Evolution of the Yidun Island Arc and the Metallogenic Model of the Pulang Porphyry Copper Deposit, Yunnan SW China (PhD Thesis) China University of Geosciences, (Beijing).
Li, J.K., Li, W.C., Wang, D.H., Lu, Y.X., Yin, G.H., Xue, S.R., 2007. Re-Os dating for ore-forming event in the late of Yanshan Epoch and research of ore-forming regularity in Zhongdian arc. Acta Petrologica Sinica 23, 2415–2422.
Li, W.C., Zeng, P.S., Hou, Z.Q., White, N.C., 2011. The Pulang porphyry copper deposit and associated felsic intrusions in Yunnan Province, Southwest China. Economic Geology 106, 79–92.
Li, W.C., Yin, G.H., Yu, H.J., Liu, X.L., 2014. The Yanshanian granites and associated Mo-polymetallic mineralization in the Xiangcheng–Luoji area of the Sanjiang–Yangtze

conjunction zone in Southwest China. Acta Geologica Sinica-English Edition 88, 1742–1756.
Liu, Y.S., Hu, Z.C., Gao, S., Gunther, D., Xu, J., Gao, C.G., Chen, H.H., 2008. In situ analysis of major and trace elements of anhydrous minerals by LA-ICP-MS without applying an internal standard. Chemical Geology 257, 34–43.
Liu, J.T., Yang, L.Q., Lü, L., 2013. Pulang reduced porphyry copper deposit in the Zhongdian area, Southwest China: constrains by the mineral assemblages and the ore-forming fluid compositions. Acta Petrologica Sinica 29, 3914–3924.
London, D., Wolf, M.B., Morgan VI, G.B., Garrido, M.G., 1999. Experimental silicate-phosphate equilibria in peraluminous granitic magmas, with a case study of Albuquerque batholith at Tres Arroyos, Badajoz, Spain. Journal of Petrology 40, 215–240.
Lowell, D.E., Guilbert, J.M., 1970. Lateral and vertical alteration–mineralization zoning in porphyry ore deposits. Economic Geology 65, 373–408.
Macdonald, R., Baginski, B., Belkin, H.E., Dzierzanowski, P., Jezak, L., 2008. REE partitioning between apatite and melt in a peralkaline volcanic suite, Kenya Rift Valley. Mineralogical Magazine 72, 1147–1161.
Meng, J.Y., 2014. The Porphyry Copper-Polymetallic Deposit in Zhongdian, West Yunnan: Magmatism and Mineralization (PhD Thesis) China University of Geosciences, (Beijing).
Meurer, W.P., Boudreau, A.E., 1996. An evaluation of models of apatite compositional variability using apatite from the middle banded series of the Stillwater Complex, Montana. Contributions to Mineralogy and Petrology 125, 225–236.
Nagasawa, H., 1970. Rare earth concentrations in zircons and apatites and their host dacites and granites. Earth and Planetary Science Letters 9, 359–364.
Pan, Y., Fleet, M.E., 2002. Compositions of the apatite group minerals: substitution mechanisms and controlling factors. Reviews in Mineralogy 48, 13–49.
Pang, Z.S., Du, Y.S., Cao, Y., Gao, F.P., Wang, G.W., Dong, Q., 2014. Geochemistry and zircon U–Pb geochronology of the Pulang Complex, Yunnan Province, China. Journal of Earth System Science 123, 875–885.
Peacock, S.M., Rushmer, T., Thompson, A.B., 1994. Partial melting of subducting oceanic crust. Earth and Planetary Science Letters 121, 227–244.
Piccoli, P.M., Candela, P.A., 1994. Apatite in felsic rocks: a model for the estimation of initial halogen concentrations in the Bishop Tuff (Long Valley) and Tuolumne intrusive suite (Sierra Nevada batholith) magmas. American Journal of Science 294, 92–135.
Piccoli, P.M., Candela, P.A., 2002. Apatite in igneous systems. Reviews in Mineralogy & Geochemistry 48, 255–292.
Pichavant, M., Montel, J.M., Richard, L.R., 1992. Apatite solubility in peraluminous liquids: experimental data and an extension of the Harrison-Watson model. Geochimica et Cosmochimica Acta 56, 3855–3861.
Prowatke, S., Klemme, S., 2006. Trace element partitioning between apatite and silicate melts. Geochimica et Cosmochimica Acta 70, 4513–4527.
Qi, L., Hu, J., Gregoire, D.C., 2000. Determination of trace elements in granites by inductively coupled plasma mass spectrometry. Talanta 51, 507–513.
Rapp, R.P., Watson, E.B., 1995. Dehydration melting of metabasalt at 8–32 kbr: implication for continental growth and crust–mantle recycling. Journal of Petrology 36, 891–931.
Rapp, R.P., Shinizu, H., Norman, M.D., Applegate, G.S., 1999. Reaction between slab-derived melts and peridotite in the mantle wedge: experimental constraints at 3.8 GPa. Chemical Geology 160, 335–356.
Rapp, R.P., Xiao, L., Shimizu, N., 2002. Experimental constraints on the origin of potassium-rich adakites in Eastern China. Acta Petrologica Sinica 18, 293–302.
Roeder, P.L., MacArthur, D., Ma, X.P., Palmer, G.R., Mariano, A.N., 1987. Cathodoluminescence and microprobe study of rare earth elements in apatite. American Mineralogist 72, 801–811.
Roegge, J.S., Logsdon, M.J., Yong, H.S., Barr, H.B., Borcsik, M., Holland, H.D., 1974. Halogens in apatites from the Providencia area, Mexico. Economic Geology 69, 229–240.
RØnsbo, J.G., 1989. Coupled substitutions involving REEs and Na and Si in apatites in alkaline rocks from the Ilĺmaussaq intrusion, South Greenland, and the petrological implications. American Mineralogist 74, 896–901.
Schisa, P., Boudreau, A., Djon, L., Tchalikian, A., Corkery, J., 2015. The Lac Des Iles Palladium deposit, Ontario, Canada. Part II. Halogen variations in apatite. Mineralium Deposita 50, 339–355.
Sen, C., Dunn, T., 1994. Dehydration melting of a basaltic composition amphibolite at 1.5 and 2.0 GPa: implication for the origin of adakites. Contributions to Mineralogy and Petrology 117, 394–409.
Sen, C., Dunn, T., 1995. Experimental modal metasomatism of a spinel lherzolite and the production of amphibole-bearing peridotite. Contributions to Mineralogy and Petrology 119, 422–432.
Sha, L.K., Chappell, B.W., 1999. Apatite chemical composition, determined by electron microprobe and laser-ablation inductively coupled plasma mass spectrometry, as a probe into granite petrogenesis. Geochimica et Cosmochimica Acta 63, 3861–3881.
Sillitoet, R.H., 2010. Porphyry copper system. Economic Geology 105, 3–41.
Streck, M.J., Dilles, J.H., 1998. Sulfur evolution of oxidized arc magmas as recorded in apatite from a porphyry copper batholith. Geology 26, 523–526.
Sun, S.S., McDonough, W.F., 1989. Chemical and isotopic systematics of oceanic basalts: implications for mantle composition and processes. Geological Society Special Publication 42, 313–345.
Tacker, R.C., Candela, P.A., 1987. Partitioning of molybdenum between magnetite and melt: a preliminary experimental study of partitioning of ore metal between silicate magmas and crystalline phase. Economic Geology 82, 1805–1826.
Tacker, R.C., Stormer, J.C., 1989. A thermodynamic model for apatite solid solutions, applicable to high-temperature geologic problems. American Mineralogist 74, 877–888.
Tepper, J.H., Kuehner, S.M., 1999. Complex zoning in apatite from the Idaho batholith: a record of magma mixing and intracrystalline trace element diffusion. American Mineralogist 84, 581–595.
Treloar, P.J., Colley, H., 1996. Variations in F and Cl content in apatites from magnetite-apatite ores in Northern Chile, and their ore-genetic implication. Mineralogical Magazine 60, 285–301.
Tsuboi, M., 2005. The use of apatite as a record of initial $^{87}Sr/^{86}Sr$ ratios and indicator of magma processes in the Inagawa pluton, Ryoke belt, Japan. Chemical Geology 221, 157–169.
Tsuboi, M., Suzuki, K., 2003. Heterogeneity of initial $^{87}Sr/^{86}Sr$ ratios with a single pluton: evidence from apatite from apatite strontium isotopic study. Chemical Geology 199, 189–197.
Tu, X.L., Zhang, H., Deng, W.F., Ling, M.X., Liang, H.Y., Liu, Y., Sun, W.D., 2011. Application for RESOlution in-situ laser ablation ICP-MS in trace element analyses. Geochimica 40, 83–98.
Wang, X.S., 2014c. Geological Setting and Genesis of Late Cretaceous Igneous Rocks and Associated Mineralization in the Southern Yidun Arc, Eastern Tibetan Plateau (PhD Thesis) Institute of Geochemistry, Chinese Academy of Sciences.
Wang, B.Q., Zhou, M.F., Li, J.W., Yan, D.P., 2011. Late Triassic porphyritic intrusions and associated volcanic rocks from the Shangri-La region, Yidun terrane, Eastern Tibetan Plateau: adakitic magmatism and porphyry copper mineralization. Lithos 127, 24–38.
Wang, X.S., Bi, X.W., Leng, C.B., Zhong, H., Tang, H.F., Chen, Y.W., Yin, G.H., Huang, D.Z., Zhou, M.F., 2014a. Geochronology and geochemistry of Late Cretaceous igneous intrusions and Mo-Cu-(W) mineralization in the southern Yidun arc, SW China: implications for metallogenesis and geodynamic setting. Ore Geology Reviews 61, 73–95.
Wang, X.S., Hu, R.Z., Bi, X.W., Leng, C.B., Pan, L.C., Zhu, J.J., Chen, Y.W., 2014b. Petrogenesis of late Cretaceous I-type granites in the southern Yidun terrane: new constraints on the Late Mesozoic tectonic evolution of the eastern Tibetan Plateau. Lithos 208–209, 202–219.
Wang, X.S., Bi, X.W., Hu, R.Z., Leng, C.B., Yu, H.J., Yin, G.H., 2015. S-Pb isotopic geochemistry of Xiuwacu magmatic hydrothermal Mo-W deposit in Zhongdian area,NW Yunnan: constrains on the sources of metal. Acta Petrologica Sinica 31, 3171–3188.
Warner, S., Martin, R.F., Abdel-Rahman, A.-F.M., Doig, R., 1998. Apatite as a monitor of fractionation, degassing, and metamorphism in the Sudbury igneous complex, Ontario. Canadian Mineralogist 36, 981–999.
Wass, S.Y., Henderson, P., Elliott, C.J., 1980. Chenical homogeneity and metasomatism in the upper mantle: evidence from rare earth and other elements in apatite-rich xenoliths in basaltic nodules from Eastern Australia. Philosophical Transactions of the Royal Society A297, 333–346.
Watson, E.B., 1979. Apatite saturation in basic to intermediate magmas. Geophysical Research Letters 6, 937–940.
Watson, E.B., 1980. Apatite and phosphorus in mantle source regions: an experimental study of apatite/melt equilibria at pressures to 25 kbar. Earth and Planetary Science Letters 51, 322–335.
Watson, E.B., Green, T.H., 1981. Apatite/liquid partition coefficients for the rare earth elements and strontium. Earth and Planetary Science Letters 56, 405–421.
Williams, S.A., Cesbron, F.P., 1977. Rutile and apatite useful prospecting guides for porphyry copper deposits. Mineralogical Magazine 41, 288–292.
Wolf, M.B., London, D., 1994. Apatite dissolution into peraluminous haplogranite melt: an experimental study of solubilities and mechanisms. Geochimica et Cosmochimica Acta 58, 4127–4145.
Wolf, M.B., London, D., 1995. Incongruent dissolution of REE-and Sr-rich apatite in peraluminous granitic liquids: differential apatite, monazite, and xenotime solublities during anatexis. American Mineralogist 80, 765–775.
Xu, W.G., Zhang, D.H., 2012. An interpretation of the role of reduced fluid in porphyry metallogenesis. Acta Geologica Sinica-English Edition 86, 495–502.
Yu, H.J., Li, W.C., 2014. Geological characteristics of Tongchanggou superlarge molybdenum polymetallic deposit of Yidun arc in Sanjiang region, China. Acta Geologica Sinica-English Edition 88, 639–640.
Yu, H.J., Li, W.C., Yin, G.H., Wang, J.H., Jiang, W.T., Wu, S., Tang, Z., 2015. Geochronology, geochemistry and geological significance of the intrusion from the Tongchanggou Mo-Cu deposit, Northwestern Yunnan. Acta Petrologica Sinica 31, 3217–3233.
Zeng, P.S., Li, W.C., Wang, H.P., Li, H., 2006. The Indosinian Pulang superlarge porphyry copper deposit in Yunnan, China: petrology and chronology. Acta Petrologica Sinica 22, 989–1000.
Zhang, W.L., Shao, J.A., Wang, R.C., Xu, X.S., Che, X.D., Yang, Y.H., 2011. Sr-rich apatite from the Dangzishan leucitite-ijolite xenoliths (Heilongjiang Province): Mineralogy and mantle-fluid metasomatism. Chinese Science Bulletin 56, 53–63.